Dust transport and deposition observed from the Terra-MODIS spacecraft over the Atlantic Ocean

Y. J. Kaufman[1], I. Koren[1,2], L.A. Remer[1], D. Tanré[3], P. Ginoux[4] and S. Fan[4] No. BAMS 1756

[1] NASA Goddard Space Flight Center, Greenbelt Maryland 20771, USA, *yoram.j.kaufman@nasa.gov*

[2] National Research Council

[3] Laboratoire d'Optique Atmospherique, CNRS, Université, de Scie. et Techniq. de Lille, Villeneuve d'Ascq, France

[4] NOAA GFDL, Princeton University, Princeton NJ

Abstract: Meteorological observations, in situ data and satellite images of dust episodes were used already in the 1970s to estimate that 100 tg of dust are transported from Africa over the Atlantic Ocean every year between June and August and deposited in the Atlantic Ocean and the Americas. Desert dust is a main source of nutrients to oceanic biota and the Amazon forest, but deteriorates air quality as shown for Florida. Dust affects the Earth radiation budget, thus participating in climate change and feedback mechanisms. There is an urgent need for new tools for quantitative evaluation of the dust distribution, transport and deposition. The Terra spacecraft launched at the dawn of the last millennium provides first systematic well calibrated multispectral measurements from the MODIS instrument, for daily global analysis of aerosol. MODIS data are used here to distinguish dust from smoke and maritime aerosols and evaluate the African dust column concentration, transport and deposition. We found that **230**±80 tg of dust are transported annually from Africa to the Atlantic Ocean, **30** tg return to Africa and Europe, **70** tg reach the Caribbean, **45** tg fertilize the Amazon Basin, 4 times as previous estimates thus explaining a paradox regarding the source of nutrition to the Amazon forest, and **120**±40 tg are deposited in the Atlantic Ocean. The results are compared favorably with dust transport models for particle radius ≤ 12 μm. This study is a first example of quantitative use of MODIS aerosol for a geophysical study.

1. Introduction

Prospero and Carlson [1972], *Prospero and Nees* [1977] and *Carlson* [1979] used meteorological observations, in situ data and satellite images (AVHRR) of dust episodes, to derive the first estimates of dust emission from Africa of 100 tg of dust for a latitude belt 5°-25°N in the summer months June to August. This estimate was done before problems with AVHRR calibration were recognized and corrected [*Holben et al.*, 1990]. Due to lack of systematic satellite measurements designed for aerosol studies, improvements in the estimates of dust emission were based mainly on models of the dust sources, emission and transport [*Tegen and Fung*, 1995; *Prospero et al.*, 1996; *Ginoux et al*, 2001]. With the launch of the first MODerate resolution Imaging Spectro-radiometer (MODIS) instrument at the end of 1999, quantitative and systematic measurements of dust transport are possible [*Gao et al.*, 2001; *Kaufman et al.*, 2002] and presented here for the Atlantic ocean.

The constant flux of dust across the Atlantic Ocean is of considerable interest. In the last 10 years the citation index reports 500 papers about or related to Saharan dust, and shows an exponential increase in the publication rate, starting from the early works of Prospero and Carlson in the 1970's (see Fig. 1). Iron contained in aeolian dust was shown to be an important micro-nutrient for ocean phytoplankton, which could contribute to fluctuation of CO_2 on climatic time scales [*Martin et al.*, 1991]. *Erickson et al.* (2003) measured, using satellite data, the effect of dust deposition on ocean productivity. Over the millennia, dust was suggested to be the main fertilizer of the Amazon forest [*Swap et al.*, 1992].

Dust particles interact with solar and thermal radiation, thus can modulate the Earth radiation balance in response to changing climate conditions or land use change [*Prospero et al.*, 2002]. It also can interact with clouds, mainly after absorbing hygroscopic material [*Levin et al.*, 1996; *Rosenfeld et al.*, 2001]. The emission of dust is associated with strong winds, generating optical thicknesses as high as 3.5 [*Pinker et al.*, 2003] in pulses of dust, each several days long [*Carlson*, 1979]. Dust also affects photololysis rates and heterogeneous reactions for ozone chemistry, by changing the concentration of UV *radiation [Dentener et al.*, 1996; *Martin et al.*, 2003].

The MODIS systematic and accurate measurements of aerosol optical thickness (τ) and the contribution to the optical thickness by the fine mode (f) [*Tanré et al.*, 1997; *King et al.*, 1999; 2003] can be used to derive the dust column concentration, flux and deposition in the Atlantic Ocean. Here we implement an approach to distinguish dust from other aerosol types using the MODIS measurements and use it to derive dust transport and deposition. This is one of the first examples of quantitative use of MODIS aerosol data for geophysical studies.

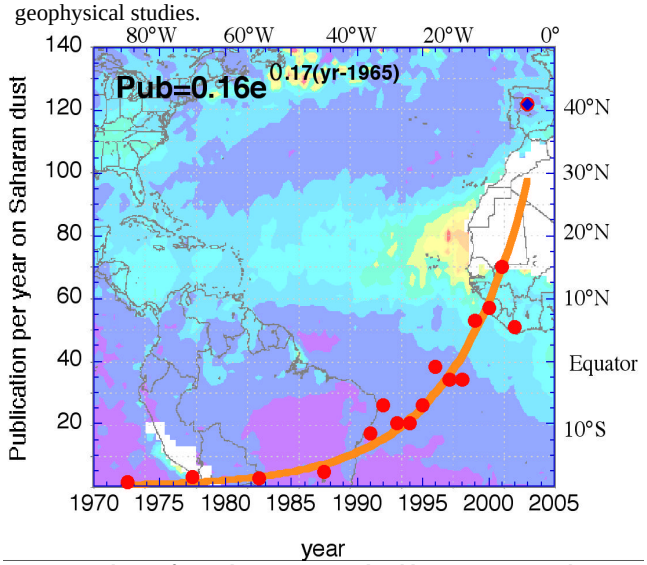

Fig. 1: Back to African dust: Exponential publication rate on Saharan dust (red dots) according to the ISI citation index, on a background of MODIS aerosol optical thickness for July 2001. The exponential growth corresponds to doubling of the publication rate every 4 years, as compared to publication rate on climate change that dopubles every 11 years [*Stanhill*, 2001]. The publication search was performed under the term "**dust and Sahar***" and is conducted on the title, abstract and key words. Note that the ISI "key words plus" introduces additional key words that generate in this case 10-20% of unrelated citations and cannot be excluded from the search. The 2003 figure is an estimate based on the first 6 months of the year.

2. Aerosol measurements from satellites

Since the early observations of African dust from the AVHRR [*Carlson*, 1979], the AVHRR was used to observe the seasonal and inter-annual variability of dust emissions [*Swap et al*.,1992; 1996; *Husar et al*., 1997; *Cakmur et al.*, 2001]. AVHRR data were used to estimate that 100 tg of dust leave Africa annually in the summer towards the Caribbean and Florida [*Carlson*, 1979] and that in the winter out of the 30 tg of dust that cross the 60°W line, 13 tg arrive to the Amazon Basin and are deposited by rain [*Swap et al*., 1992]. This analysis of the AVHRR data allowed *Swap et al*. [1992] to suggest that recycling of nutrients in the biologically rich Amazon Basin over thousands of years time scales depends on dust transport and deposition from the biologically deprived African Sahara. However they pointed out that 50 tg are needed to keep the Amazon fertilized, creating a paradox of the missing nutrients.

Despite these insights gained from the AVHRR, a spaceborne sensor not designed originally for aerosol measurements, the accuracy of the AVHRR data regarding aerosol is limited. AVHRR was not used to distinguish between dust, smoke, pollution, stratospheric aerosol or sea salt, therefore the interpretation of aerosol measurements as dust depends on outside knowledge of the aerosol type and composition that is often incomplete. For example *Swap et al.* [1996] found differences of factor of 3 in dust deposition between the end of the 1980's and the beginning of the 1990's, recognizing that their conclusions can be affected by the presence of stratospheric aerosol, but did not have the tools to correct for it. Analysis of the AVHRR data created therefore the illusion that maximum dust transport from Africa occurs in February (Swap et al 1996), while here we show that the maximum is in the summer, as suggested already by Carlson and Prospero in the 1970's. The illusion stems from considering the mixture of smoke from the Sahel with dust from the Sahara in February as pure dust. In June-July biomass burning moves south and is not mixed with dust emitted from the Sahara. Only recently the AVHRR aerosol data became better calibrated and validated [*Ignatov and Stowe*, 2002]. Note that Prospero et al. [1981] did find higher dust concentration in in situ measurements at surface level

TOMS UV measurements were found to be sensitive to dust and smoke due to their absorption of sunlight reflected in the UV by atmospheric gases [*Hsu et al.*, 1996; *Herman et al.*, 1997]. TOMS can distinguish between the absorbing dust and smoke from pollution and sea salt that do not absorb sunlight [*Torres et al.*, 2002]. TOMS data were used to identify globally the location and geomorphological characteristics of dust sources [*Prospero et al*., 2002], their physical and optical characteristics [*Ginoux and Torres*, 2003], and to verify the location of dust sources estimated in the model using an independent scheme [*Ginoux et al*., 2001]. The African dust sources were found to be located in sparsely populated areas, north of 15°N, indicating that most if not all of African dust is of natural origin [*Prospero et al*., 2002]. Together with the Aerosol Robotic Network (AERONET) of sun sky radiometers TOMS data were used to test and improve dust emission and transport models [*Chin et al*., 2002; *Ginoux et al.*, 2003], and to initialize dust transport models [*Alpert et al*., 2002].

Several authors used TOMS aerosol index to investigate the variability of dust distribution on a seasonal [*Cakmur et al*., 2001] and inter-annual [*Moulin and Chiapello*, 2002; *Ginoux et al*., 2003] scales. *Cakmur et al.* [2001] showed the seasonal cycle using TOMS and AVHRR, with maximum dust concentrations in the summer, and explained the much sharper annual cycle observed by TOMS than by AVHRR by the variation of the dust altitude (close to the surface in the winter months – *Chiapello et al.*, 1995). While TOMS aerosol index is proportional both to the dust concentration and to the height of the dust layer, and thus the strength of the molecular reflection of UV radiation under the dust, AVHRR is only dependent on the dust concentration.

Chiapello et al. [1999a] compared TOMS aerosol index with ground based measurements, showing excellent agreement in Barbados and lesser agreement in Capo-Verde, where the seasonal variation of the vertical distribution causes high dust concentration near the surface in the winter months, while in the summer the dust flows above the area [*Karyampudi et al*., 1999] on its way to Barbados, as was shown from Meteosat by *[Jankowiak and Tanré*, 1992]. The variation in spatial, seasonal and inter-annual dust concentration observed from *Meteosat [Jankowiak and Tanré*, 1992], generated interest in the origin of this variation, e.g. correlation with the North Atlantic oscilations [*Moulin et al.*, 1997a] and in its use to measure the climatic temperature response to the presence of dust [*Alpert et al.*, 1998]. Conversion of the AVHRR, TOMS or METEOSAT data to dust column loading depends on the quality of calibration, and validity of assumptions on the aerosol scattering properties and height in the case of TOMS.

Measurements from the MODIS instruments provide new opportunities. MODIS began collecting data in April 2000 and May, 2002 from Terra and Aqua spacecraft respectively. Special emphasize is given to on-board calibration facilities, lunar observations and detailed analysis of the calibration time series on the ground [*Barnes et al.*, 1998]. MODIS measured spectral radiances from 0.47 μm to 2.1 μm are used to characterize the global aerosol. The aerosol characteristics are derived over the oceans [*Tanré et al*., 1997] and land [*Kaufman et al.*, 1997] using independent algorithms. Over oceans, the MODIS aerosol algorithm uses the measured 500m resolution radiance from six MODIS bands (550-2100 nm) to retrieve the aerosol information. Specifically, in cloud-free, glint-free ocean scenes [*Martins et al.*, 2002], MODIS retrieves at a 10 km resolution: the aerosol optical thickness at 550 nm, τ, the fraction of τ contributed by the fine (sub-micron size) mode aerosol, f, and the effective radius of the aerosol, R_{eff} [*Tanré et al.* 1997]. These three pieces of information were chosen using an information content analysis [*Tanré et al*., 1996]. Aggregation of the MODIS aerosol information from the 500 m pixels to the 10 km product, allows rigorous cloud screening, avoiding data gaps and still generates large enough statistics for a stable and accurate product. The MODIS derived aerosol properties were validated before [*Tanré et al*., 1999] and after [*Remer et al.*, 2001] the launch of Terra. In agreement with theoretical error analysis [*Tanré et al* 1997], the aerosol optical thickness is derived with an error of $\Delta\tau = \pm 0.03 \pm 0.05\tau$. The errors were found to be mostly random with very little bias remaining for large statistics of data [*Remer et al.*, 2002]. For aerosol dominated by dust a bias of about +10% was noticed. Figure 2 shows an example of the MODIS observations of a dust storm off the coast of Africa observed from Terra and Aqua, and Fig. 3 the monthly variation of dust and smoke over the Atlantic Ocean.

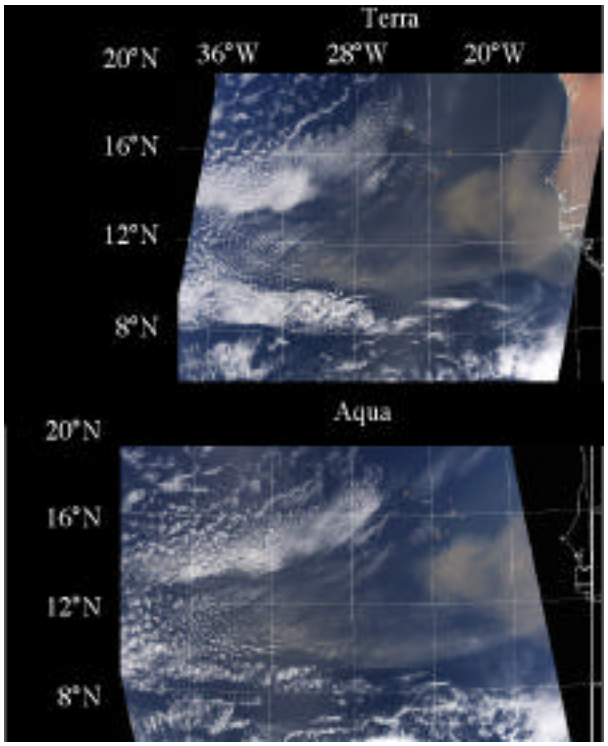

Fig. 2: Examples of MODIS observation of dust storms off the coast of Africa for Terra (10:30 am local time) and Aqua (1:30pm local time) for May 1st, 2003. The image is a composite of visible channels (0.47, 0.55 and 0.66 μm for the blue green and red colors). The dust storm moved 120 kms between the Terra and Aqua observations, corresponding to wind speed in the dust layer of 11m/s.

3. Dust column concentration

The dust column concentration is calculated using MODIS standard measurements of the aerosol optical thickness, τ at 550 nm, and the fraction of τ contributed by the fine aerosol, f, in the dust belt to distinguish dust from maritime and biomass burning aerosol [*Kaufman et al.*, 2002]. Note that the meaning of the fraction - f is that the optical thickness of the fine aerosol is $f\cdot\tau$, and of the coarse aerosol $(1-f)\cdot\tau$. The aerosol optical thickness measured by MODIS is composed in the present case of maritime, dust and anthropogenic aerosol (mainly biomass burning):

$$\tau = \tau_{maritime} + \tau_{dust} + \tau_{anthropog} \quad (1)$$

Fine aerosol is found in different proportions in the maritime aerosol, dust or anthropogenic aerosol. *Kaufman et al.* [2002] suggested that the much higher fraction of fine particles in anthropogenic aerosol as compared to dust or maritime aerosol can be used to distinguish between them in regions with high anthropogenic or dust concentrations. The procedure to do so follows:

First we use the MODIS aerosol measurements in regions of concentrated dust, in regions of concentrated smoke, and in regions with mostly maritime aerosol in the Southern Atlantic (0-30°S) to find the fraction of fine aerosol for each of these aerosol types as reflected in the MODIS data. The results are:

$$f_{maritime}=0.5\pm0.05,\ f_{dust}=0.5\pm0.05 \text{ and } f_{anthropog}=0.9\pm0.05 \quad (2)$$

The fraction of fine maritime aerosol of 0.5 agrees with analysis of AERONET data for the baseline maritime aerosol derived for the Pacific and Atlantic oceans [*Kaufman et al.*, 2001]. The fraction of fine aerosol for dust is much larger than expected from AERONET analysis. Dust non-sphericity [*Dubovik et al.*, 2002; *Mishchenko et al.*, 1997], presently not accounted for in the MODIS analysis [*Remer et al., 2002*] generates spurious high fraction of fine aerosol. Despite this fact, consistent analysis, in which the fraction f is determined from the MODIS data and used in turn to calculate fraction of anthropogenic aerosol from the MODIS data themselves, should generate the correct optical thicknesses of the individual components: $\tau_{maritime}$, τ_{dust} and $\tau_{anthropog}$. Therefore, the fraction f, is given by:

$$f = [0.5\tau_{maritime} + 0.5\tau_{dust} + 0.9\tau_{anthropog}]/\tau \quad (3)$$

and can be used to deduce the dust optical thickness, τ_{dust}:

$$\tau_{dust} = \tau(0.9-f)/0.4 - \tau_{maritime} \text{ where } 0.9\geq f\geq 0.5 \quad (4)$$

We found $\tau_{maritime}$ = 0.06±0.005 based on the analysis of MODIS data in the clear Southern Atlantic region (0°-30°S). The uncertainty of 0.005 is estimated for the regional annual average optical thickness and individual monthly averages are expected to be significantly different. The value of 0.06 also agrees with the analysis of baseline aerosol using AERONET [*Kaufman et al.*, 2001], and with the analysis of natural aerosol in INDOEX of $\tau_{maritime}$ = 0.07 [*Ramanathan et al*., 2001]. For an error of 10% [Remer et al., 2002] in τ and 10% in $\tau(0.9-f)/0.4$ we get using Monte Carlo calculations 10-15% error in τ_{dust} for τ_{dust}>0.1 (see appendix).

Figure 4 shows the latidudinal dependence of the monthly average aerosol optical thickness and its division into maritime, dust and anthropogenic components. Three longitudinal cross sections across the Atlantic ocean are shown. Anthropogenic aerosol is maximum in February due to influx of biomass burning smoke from the Sahel, and is minimal in July. It is larger at 70-80°W due to pollution and smoke from the Americas.

Figure 5 shows the monthly average dust optical thickness and total optical thickness, averaged over the dust belt (0°-30°N). The total optical thickness includes also maritime and anthropogenic (mainly biomass burning) aerosol. Since strong winds are responsible for the dust mobilization and transport over the Atlantic, it can be anticipated that the dust component of the optical thickness will be influenced more by the winds than the total optical thickness. The kinetic energy used to release dust particles is proportional to the wind speed to the second power, while dust optical thickness, for a given emission rate is inversely proportional to the wind speed. Therefore we can expect, to a first order, a linear dependence of the dust concentration with the wind speed. And in fact, for the cross section near the African coast, the correlation between the wind westward component and the average optical thickness increases from 25% for the total aerosol optical thickness to 82% for the dust component (Fig. 5). Note that the process of smoke generation from man-made fires in Africa is not expected to produce smoke in proportionality to a power of the wind speed. The analysis shows that the maximum dust concentration near the coast of Africa occurs in the summer (June-August).

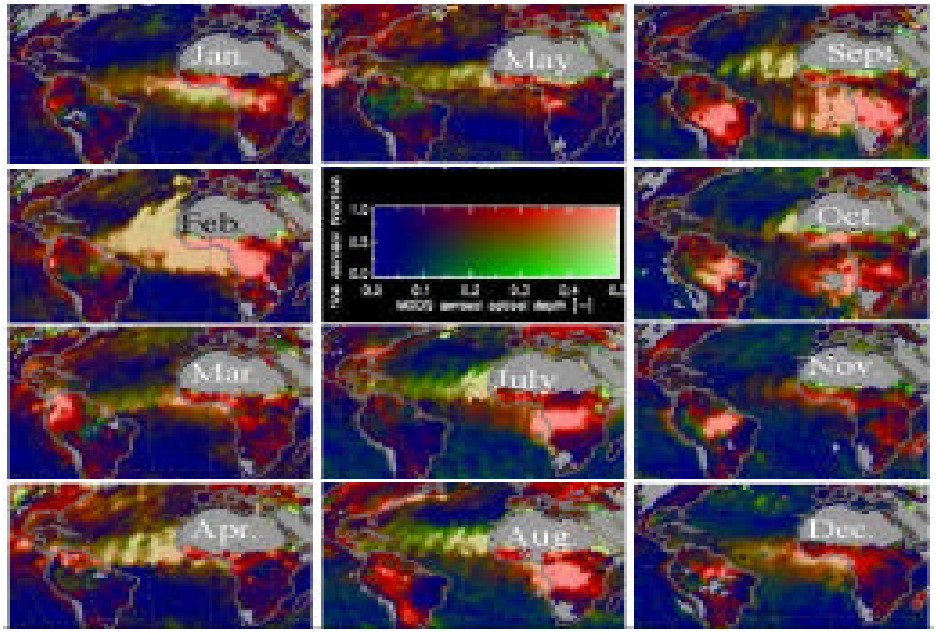

Fig 3: MODIS aerosol monthly composites for 2001. Each composite is for the 15th of each month ± 5 days to find enough cloud free regions. Data for June are not shown since no MODIS data were available during the middle of the month. The color bar is located instead. The color bar was constructed so that blue represents clean conditions, aerosol optical thickness <0.1, green and red show higher optical thickness corresponding to the coarse (green) and fine (red) modes. Therefore pure dust is green, and pure smoke or pollution red. Note that the color of the aerosol emitted from Africa changes from mixed red and green in January through April, to green in July-August. Biomass burning occurs in the Sahel during January-March, and moves to Southern Africa for July-August, when it is separated from the dust flow.

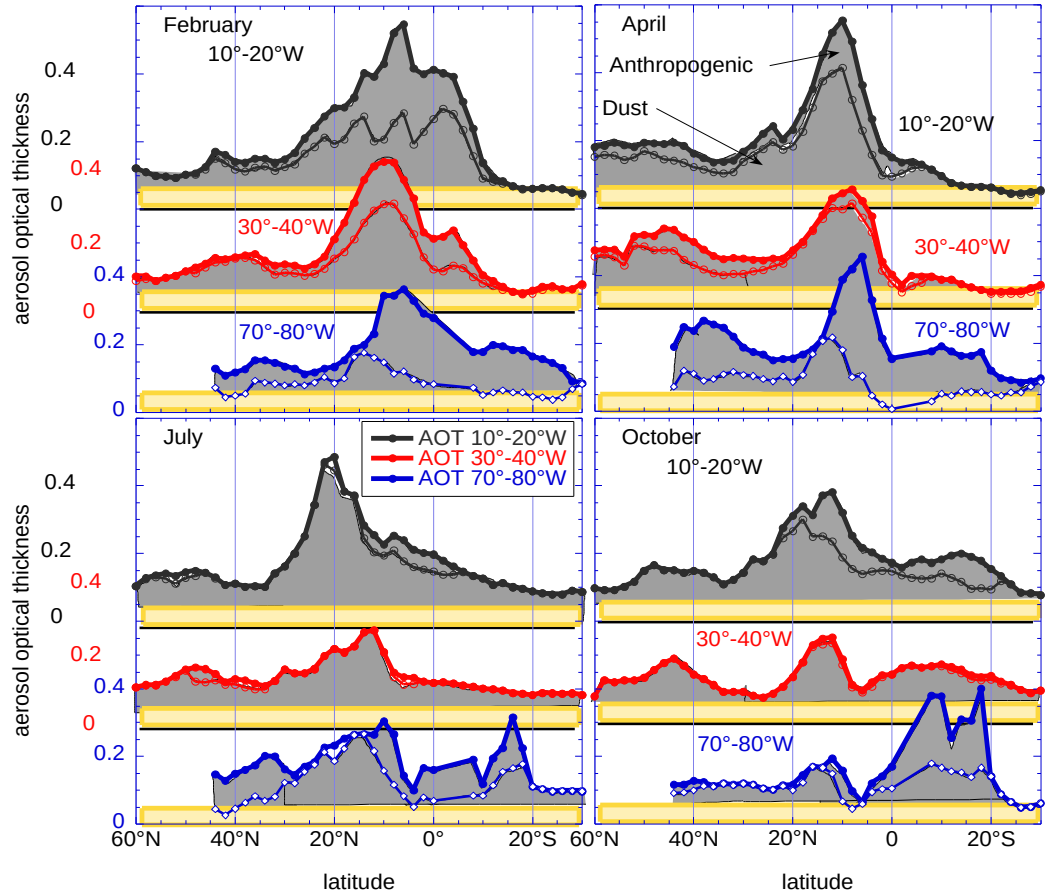

Fig. 4: Latidudinal dependence of the monthly average aerosol total optical thickness (thick line), the anthropogenic portion (uniform gray area), dust portion (granuled area) and the maritime aerosol (yellow area) for four months (February, April, July and October). The optical thickness and its components are computed from the MODIS aerosol measurements (eq. 1-4). Results are shown for longitudinal cross section at 10-20°W, 30-40°W and 70-80°W, averaged over the ocean only. The anthropogenic aerosol is maximum in February due to influx of biomass burning smoke from the Sahel, and minimal in July. It is larger at 70-80°W due to pollution and smoke from the Americas.

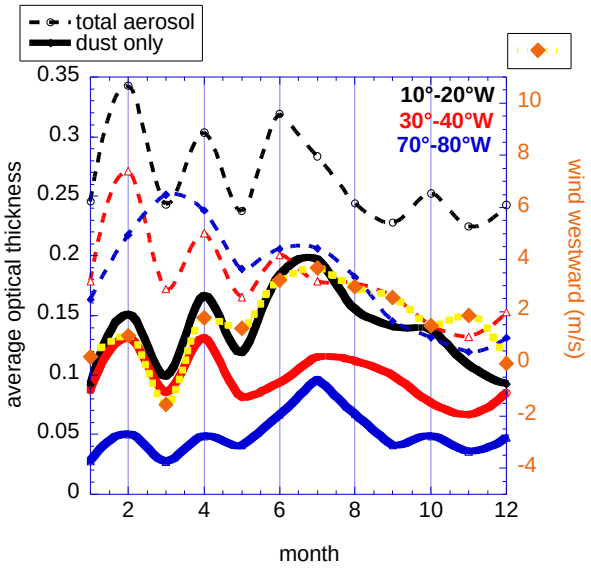

Fig. 5: Monthly average dust optical thickness (solid lines) and total optical thickness (dashed lines) averaged on the dust belt (0°-30°N), for each month of 2001. 3 longitudinal cross sections are shown: near the African coast (10°-20°W - black), near the South American coast (30°-40°W - red) and in the Caribbean (70°-80°W - blue). The monthly average dust optical thickness at 10°-20°W (solid black) is compared with the monthly mean westward component of the wind velocity (yellow-orange line) derived from NCEP reanalysis data. The winds were chosen from 700mb for May-September [*Carlson and Prospero*, 1972] and 850mb for October-April, based on analysis of *Chiapello et al.*, [1995] and *Cakmur et al.*, 2001]. Note that during June the data are available for only one week.

The dust particles are transported westward across the Atlantic Ocean by the middle level easterly jet and sometimes North by the anticyclone over the Azores or Canaries Islands. The latitudinal variation of the dust belt is controlled by the movement of the West African mid-tropospheric jet [*Carlson and Prospero*, 1972; *Hastenrath*, 1986] which occupies its northernmost position (20°N) in the summer. Figure 6 shows the latitudinal movement of the aerosol optical thickness during the three years of MODIS observations. It also shows the longitudinal transport and deposition of the dust (decrease in the optical thickness). Location of the maximum dust concentration varies from the Equator in the winter (December-February) to 20°N in July, transporting the heaviest dust to the Caribbean islands and Florida [*Prospero and Carlson*, 1972]; *Prospero et al.*, 1999].

The inter-annual variability of the dust optical thickness is also shown in Figs 7 and 8. Though for specific months (Fig 7) there is variability from year to year, the results show little difference between the whole of 2001 and 2002 (the only MODIS full years of data) of 5% in the average optical thickness and 14% in the derived dust column concentration.

4. Dust transport and deposition

The dust column concentration, $M_{dust}(gr/m^2)$, is derived from the dust optical thickness, τ_{dust}. In the Appendix we derive the ratio of the dust column mass to its optical thickness:

$$M_{dust} / \tau_{dust} = 1.33\rho R_{eff}/Q = 2.7 \pm 0.4 gr/m^2 \quad (5)$$

where τ_{dust} is at 0.55 μm, ρ is the dust density, Reff is the dust particle effective radius and Q is the light extinction efficiency. Using Eqs.4 and 5 we get:

$$M_{dust} = 2.7[\tau(0.9-f)/0.4 - \tau_{maritime}] \quad gr/m^2 \quad (6)$$

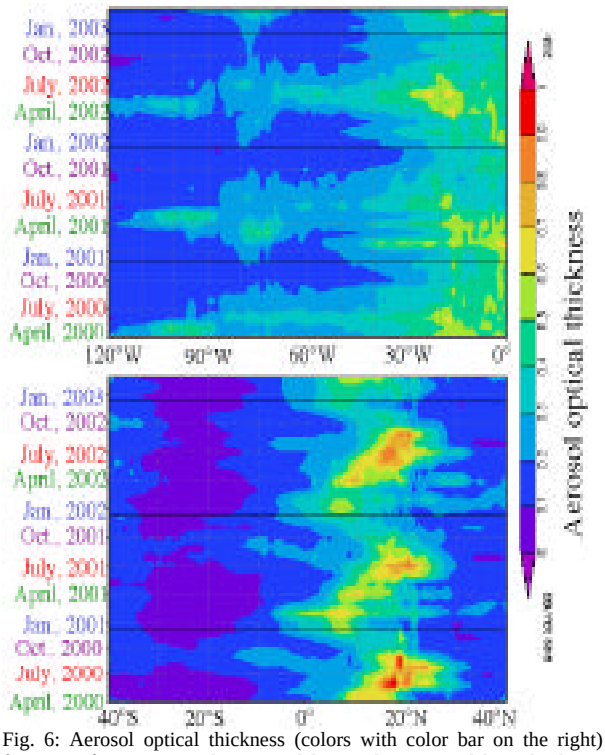

Fig. 6: Aerosol optical thickness (colors with color bar on the right) as function of time (vertical axis) and longitude (top) and latitude (bottom). The figures are averaged over 5°-20°N and or 15°-20°W respectively. The top figure shows the annual dust transport westward from Africa to the Caribbean and deposition in the Atlantic Ocean, observed as a reduction in the optical thickness. The lower figure shows the high dust emissions in May –September, with its maximum moving North from 7°N in February to 20°N in September. The images are constructed from monthly average data on the MODIS on line web site:
http://daacdev2.gsfc.nasa.gov/daac-bin/trmm_analysis_html.pl?pid=modis

The NCEP reanalysis data set is used to calculate the dust transport. The winds are chosen for 700mb (~3 km) for May-September as suggested by *Carlson and Prospero* [1972] and 850mb (1.5 km) for October-April, based on analysis of *Chiapello et al.*, [1995] and *Cakmur et al.*, [2001]. Before applying the wind field data to the aerosol field, we performed several tests of the applicability of the wind field to the problem.

In Fig. 9 we plot the correlation between the westward component of the wind speed and the aerosol optical thickness in Capo Verde, downwind from the African dust. The correlation is high at altitudes of 2.6-5 kms during the summer months of May through September. The correlation between the wind and dust optical thickness time series during the summer months is plotted in Fig, 10. The correlation coefficient is drawing a vertical profile of the wind driven aerosol concentration: dust at the layer of 3-5 km and sea salt in the lowest 500m. This correlation profile, serving as a "virtual lidar" concurs with the height selection for the wind field.

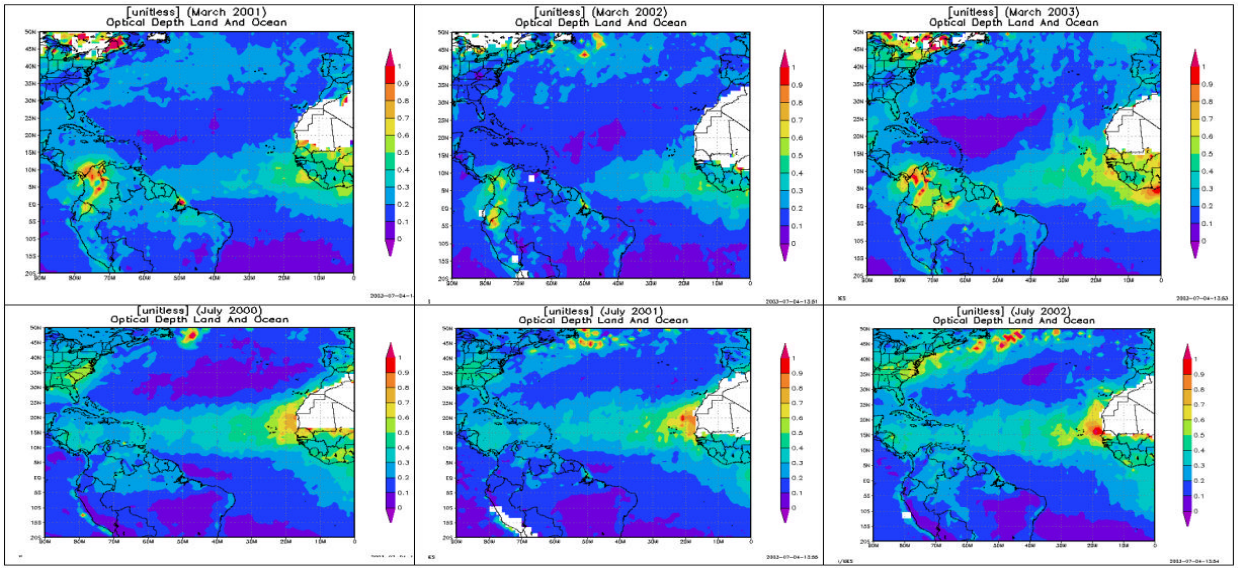

Fig. 7: Spatial distribution of the aerosol optical thickness in the Atlantic dust belt. The maps are for 20°S-50°N and 0°-90°W for March 2001-2003 and July 2000-2002. Images were produced using the on line aerosol data at http://daacdev2.gsfc.nasa.gov/daac-bin/trmm_analysis_html.pl?pid=modis. There is little variability observed from one year to another. In March dust and smoke transport is strongest in 2003 with larger Northbound component, and weakest in 2002. In July the transport is maximum is similar in the 3 years. Note the dense pollution emitted from the East coast of the US in 2003. Overall the difference in average optical thickness between 2001 and 2002 was only 5%.

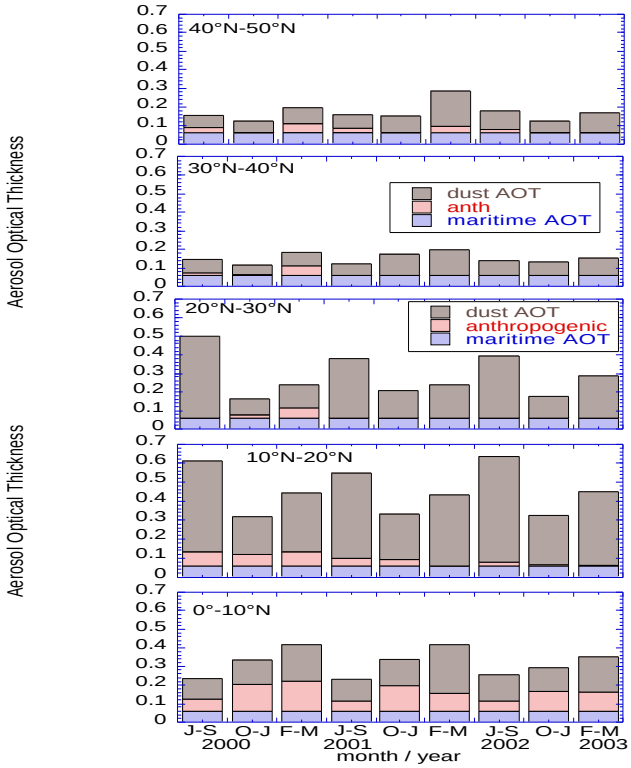

Fig. 8: Four months average aerosol optical thickness from June 2000 till March 2003 classifid as maritime (blue stripes - τ defined as 0.06), anthropogenic) (red mash) and dust (brown mash) calculated from the monthly averaged optical thickness and the fraction of the optical thickness due to the fine aerosol. These data are taken from http://daacdev2.gsfc.nasa.gov/daac-bin/trmm_analysis_html.pl?pid=modis. The separattion to maritime andhropogenic and dust componenets was done using eq. (4).

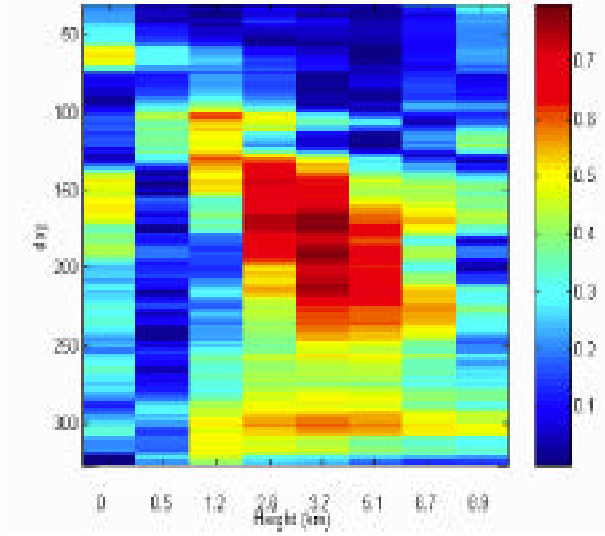

Fig. 9: Correlation between the westward component of the wind speed taken from the NCEP reanalysis and the aerosol optical thickness measured by AERONET in Capo Verde. The correlation (color bar on the right) is calculated for two months running sequences of wind and aerosol data only with aerosol optical thicknesses for Angstrom exponent <0.3. Note the high correlations between the aerosol optical thickness and the wind speed at altitudes of 2.6-5 kms during May throiugh September. 160 measurements were used in the analysis.

In Figure 11 we look again on the correlation of dust optical thickness with the profile of the wind, but using this time the MODIS derived dust concentration, for several latitude bands. For latitudes with the highest dust concentration we also see the highest correlation with the wind speed. Note that in the winter there is no clear correlation with dust concentration in a given height, though the dust is expected to be closer to the surface as suggested by *Chiapello et al*., [1995].

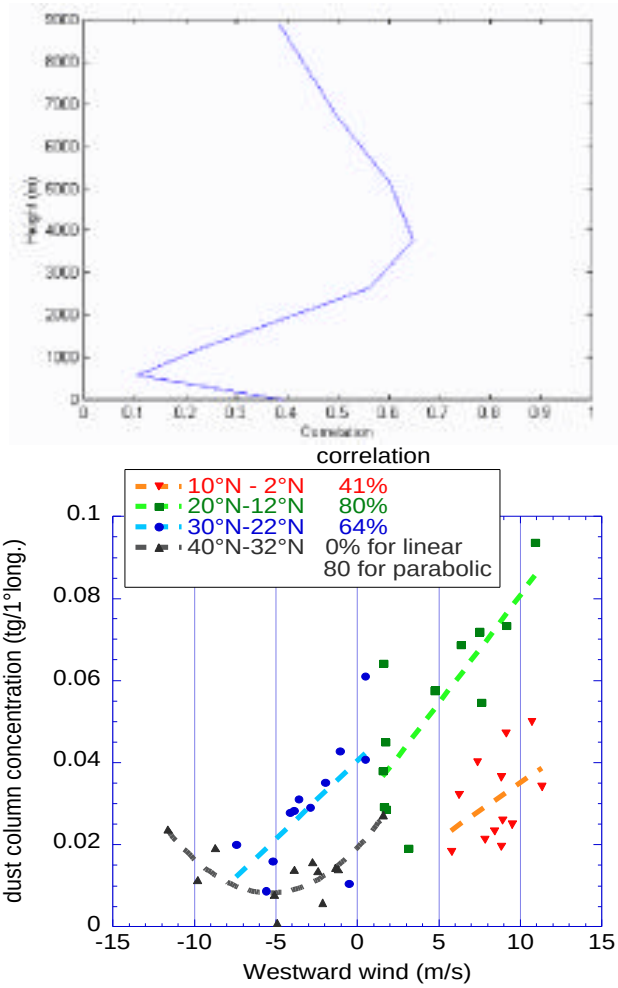

Fig. 10: Correlation between the wind and dust optical thickness time series measured in Capo Verde during the summer months. 115 measurements were used in the analysis. The correlation coefficient is drawing a profile of the wind driven aerosol. Dust at the layer of 3-5 km and sea salt in the lowest 500m. This correlation profile serves as a virtual lidar that draws the concentration of the wind driven aerosol (after *Koren et al.*, in preparation).

Fig. 11: Scatter plots of the monthly average dust column concentration as a function of the monthly average Westward wind speed for four latitide ranges as indicated, and a longitudinal cross section at 10°-20°W. Each point represents a monthly averge. The correlation bettween the wind speed and the dust concentration varies between 80% for the region with the highest dust concentration to zero for linear corrletion at 30°-40°N.

The actual wind speed can be tested against the rate of progression of the dust across the Atlantic Ocean, observed from two consequent MODIS observations, 3 hours apart one on Terra and second on the Aqua satellites. Example of the analysis is shown in Fig. 12. The direction and speed of the dust transport is calculated by finding the shift of the Terra image relative to Aqua image. The direction of transport corresponds to altitude of 700 mb (3 km), however the NCEP wind speed is 15% slower than the rate of progression of the dust. Analysis of 4 such cases (Koren et al in preparation) shows that near the shore the NCEP winds speed underestimates the dust westward progression by 15% in the 5°-25°N dust belt. Further from the shore the winds did not match the dust progression analysis at all [*Koren et al., in preparation*]. Therefore the dust transport will be calculated only in the vicinity of the continents.

The flux, F, of dust transported from Africa at 15°W is calculated by applying the monthly average westward wind speed, W(m/s), to the monthly average dust concentration, M_{dust} (g/m^2), and the longitudinal length, L (m), of the segment through which the flux is being computed (see discussion for the use of mointhly mean values):

$$F(15°W) = M_{dust}(15°W)W(15°W)L \quad g/s \qquad (9)$$

The units then can be transformed to tg/month and applied also to the 35°W and 75° W transections. The values of the seasonally averaged winds are shown in Table 1. The dust transport is summarized for the same two seasons in Table 2. The uncertainty in the fluxes reported in Table 2 result from uncertainty of ±30% in the dust concentration and uncertainty of ±15% in the wind speed near the continents, resulting in total uncertainty of ±35%. Deposition calculations are based on flux diversion. We assume that the errors in the flux are correlated and therefore the errors in deposition rates are still 35%.

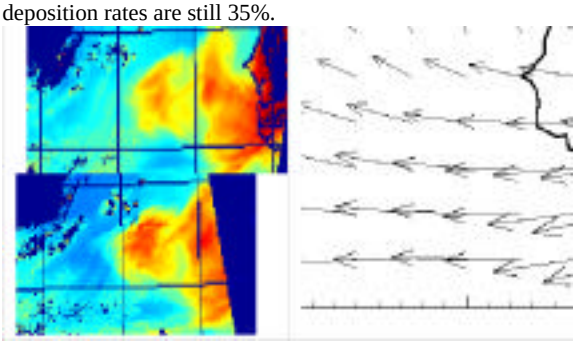

Fig. 12: Dust classified in the MODIS images from Terra and Aqua images of Fig. 2 for May 1st 2003 (images on the left). The westward shift of the dust plume between the two observations taken 3 hours apart is 120 km, corresponding to wind speed of 11 m/s. The NCEP winds for that day were 7.5 and10 m/s for 850 (1.5 km) and 700mb (3 km) respectively. The MODIS data show direct westward progression. This wind direction corresponds to NCEP winds at 750mb (interpolated between 850 and 700) with wind speed of 9.2 m/s 15% smaller. Right: NCEP wind field at 700 mb.

Table 1: Average Westward component of the wind velocity (m/s) at 850 mb for Oct.-April and 700 mb for May-Sept. from the NCEP reanalysis data for two parts of the year and for 3 longitudinal cross sections across the Atlantic Ocean

Period	10°-20°S	0°-8°S	0°-10°N	10°-20°N	20°-30°N	30°-40°N	40°-50°N
10°-20°W – West African coast							
Oct-April	5.4	5.1	3.9	4.2	1.2	-2.5	-5.3
May-Sept	3.5	4.1	6.9	9.9	-0.8	-4.1	-6.9
30°-40°W – East South American coast							
Oct-April	5.4	7.9	8.2	6.5	1.6	-4.7	-7.6
May-Sept	2.9	5.2	6.1	7.8	1.9	-4.3	-9.5
70°-80°W – Caribbean							
Oct-April			2.0	7.3	1.1	-6.4	
May-Sept			6.0	7.0	0.7	-4.6	

Overlall **230±80** tg of dust are transported annualy from Africa at 20°S-30°N. From that **30±10** tg return east to Africa and Europe at 30°N-50°N, **120±40** tg are deposited in the Atlantic Ocean, **45±15** tg reach the Amazon Basin and **70±25** tg arrive to the Caribbean. About **50±30** tg are observed to return from the Americas at 40°N-50°N. This last estimate is the most uncertain: the strong winds at 40°N-50°N may increase the maritime contribution above the baseline optical thickness of 0.06, generating artificially large dust optical thickness; part of this dust can come from East Asia through the North America; and the winds are taken in the moddle of the ocean where they are most uncertain. Table 2 and Fig. 13 summarizes these fluxes as a function of their geographic position.

The flux to the Amazon of 45±15 tg, much larger than in the analysis of *Swap et al.*, [1996] may explain the paradox that they found between the low estimate of dust deposition in the Amazon of 13 tg and the order of magnitude larger estimate of the flux needed to sustain the forest. The present estimates of dust transport are more in line with the earlier estimates of *Prospero and Carlson* [1972].

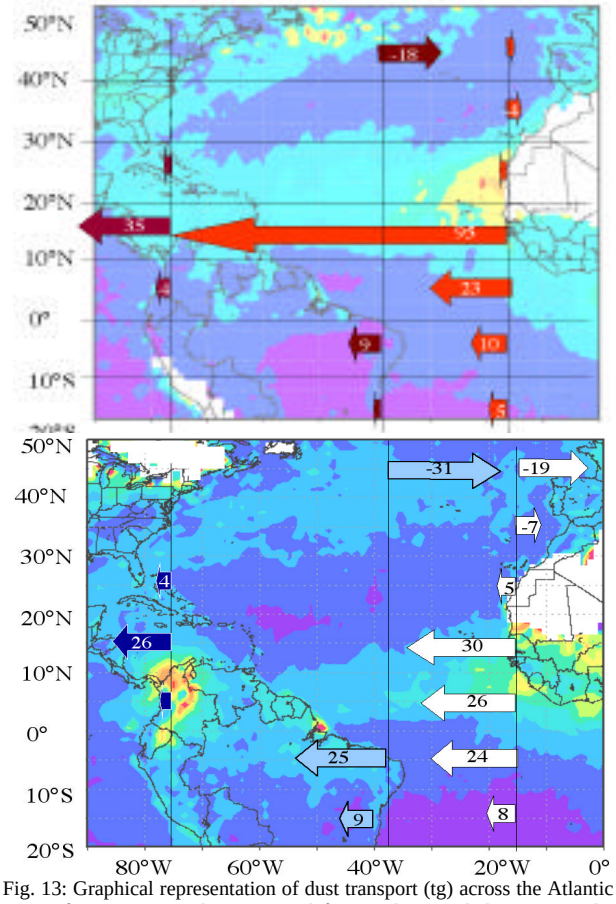

Fig. 13: Graphical representation of dust transport (tg) across the Atlantic Ocean for May-September (top) and for October-April (bottom) on the background of MODIS image from July and March 2001 respectively. The dust transport is given for longitudinal cross-sections at 15°W, 35°W and 75°W, near the continents where the wind field is more reliable.

The results of dust deposition are compared with the models of *Prospero et al.* [1996], *Ginoux et al.* [2001, 2003] and *Gao et al.* [2001, 2003] in table 3 and Fig. 14. A good agreement is found between the dust deposition in the Atlantic Ocean as observed by MODIS and calculated in the Ginoux et al. model and the Gao et al. model for dust radii < 12 µm. The MODIS seasonal deposition is very similar to the seasonal deposition derived from the Ginoux et al. model.

Table 2: dust flux through the longitudinal cross sections for each segment of 10° latitude in tg of mass of dust for the indicated period.

Period	20°-10°S	10°S-0°	0°-10°N	10°-20°N	20°-30°N	30°-40°N	40°-50°N	Total
10°W-20°W - West African coast annual flux **195** tg/yr								
Oct-April	8	24	26	30	5	-7	-19	66
May-Sept.	5	10	23	95	2	-4	-2	129
30°W-40°W – Amazon & N. America annual flux **45** & **-50** tg/yr								
Oct-April	9	25					-31	
May-Sept	2	9					-18	
70°W-80°W– Caribbean annual flux **70** tg/yr								
Oct-April			3	26	4	-5		28
May-Sept			4	35	2	0		41

Table 3: Comparison of dust deposition during 4 seasons for 0°-40°N between MODIS data, the model of *Gao et al.* [2003], the GOCART model of *Ginoux et al.* [2001, 2003], the results of *Gao et al.* [2001] and *Prospero et al* [1996]. *Gao et al.* [2001] dust deposition were reconstructed from their iron deposition calculations for 3.5% fraction of iron in the dust. Except for *Prospero et al* [1996], the results are given for 2001.

	Gao et al. [2003]		*Ginoux et al.* [2001	**MODIS**	*Gao et al.* [2001]		*Prospero et al* [1996]
Season	0.2-6 µm	0.2-12 µm	(tg)	**(tg)**	Iron (tg)	Dust (tg)	
Spring	19	42	29	**16**	1.4	41	
Summer	39	90	48	**51**	2.5	72	
Fall	19	39	41	**34**	2.3	66	
Winter	18	40	24	**17**	0.9	25	
Total	95	210	143	**117**	7	204	170

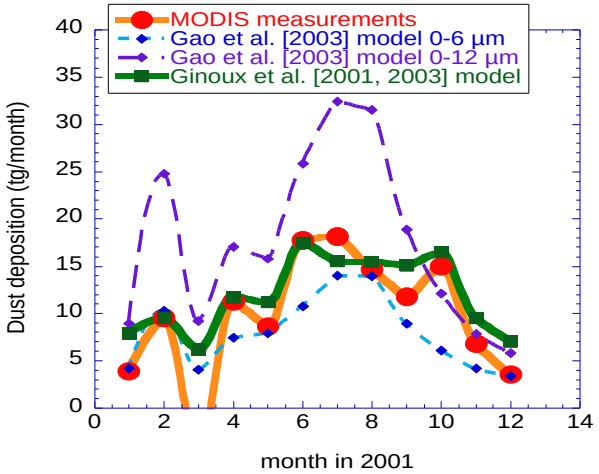

Fig. 14: Dust deposition rates (tg/month) derived from MODIS measurements and calculated by the chemical transport models of *Ginoux et al.* [2001, 2003] and *Gao et al.* [2003] for the region (0°-40°N).

5. Discussion

The error analysis did not account several processes that can introduce additional uncertainty and are addressed here:

a) Monthly averaging: The first issue is the calculations of the dust fluxes across the longitudinal cross sections. The fluxes are calculated as the product of the monthly mean westward component of the wind and the dust mass column concentration. This approach can be valid if the correlation between dust concentration and wind speed does not affect the monthly flux. Therefore we need to check if the flux given by eq. 8, F_M, for the product of the monthly averages $<M_{dust}>$ for dust concentration and <W> for average westward component of the wind, is equal to the accurate estimate using the daily data of MODIS dust concentration and winds. Therefore defining:

$$F_M = <M_{dust}><W>L \quad \text{and} \quad <F_D>= <M_{dust}W>L$$

we need to check if: $$F_M = <F_D> \qquad (11)$$

In Fig. 15 we compare the monthly average wind speed <W> with wind speed weighted by the dust concentration (for simplicity the aerosol optical thickness was used as the weighting factor:

$$W_w = <M_{dust}W>/<M_{dust}> \qquad (12)$$

Thus if $W_w \approx <W>$ then $F_M \approx <F_D>$. The result, shown for four pressure levels, show that $W_w \approx <W>$ on average withn 5%.

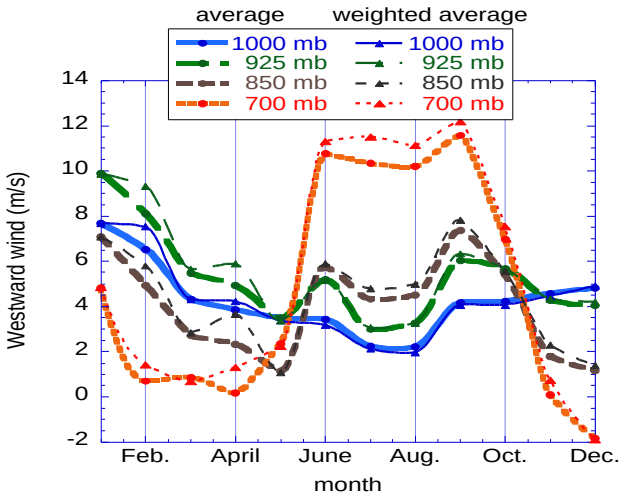

Fig. 15: Annual cycle of the monthly average westward component of the wind for 4 pressure levels. The average wind speed was calculated by two methods: simple monthly average around the satellite pass time of 9:30 GMT for the longitude of 15°W, and weighted average, with the weight being the aerosol optical thickness measured by MODIS.

b) Maritime aerosol: The second issue is the use of constant maritime aerosol optical thickness of 0.06 for 550 nm. There were several publications that indicated the dependence of maritime aerosol extinction coefficient on the wind speed. Recently *Smirnov et al.* [2003] used AERONET data to relate the column optical thickness to the wind speed. They found, for the data from 2001 for Midway Island that the optical thickness at 500 nm is correlated with the surface wind speed as:

$\tau(500\ nm) = aW+b$, a=0.0068, b=0.056 correlation=0.37 (13)

where the wind speed is averaged on 24 hr. The value of b is also affected by non-maritime transport. The most common value of the optical thickness was found to be 0.06, as used here. For range of 2-10 m/s it corresponds to change in τ of 0.05. *Smirnov et al.* [2003] reviewed other studies and deduced from them values of ranging from a=0.002 to 0.008. In the present analysis we found that the average surface annual wind speed in the three longitudinal cross sections is 4.1±0.8, 5.5±1 and 3.8±0.6 for 15°W, 35°W and 75°W respectively. This corresponds to variation in the maritime optical thickness of +0.01 from 15°W, to 35°W and –0.01 from 35°W to 75°W. Therefore we do not expect any change in the total deposition in the Atlantic ocean but a shift of 5% of the total deposition of 115 tg from the Western Atlantic to the Eastern Atlantic.

c) Diurnal cycle: A dust persistent diurnal cycle could generate an error in the monthly and annual estimates presented here. It was already reported [*Kaufman et al.*, 2000] that on global basis the Terra measurements at ~10:30 am or the Aqua measurements at 1:30 pm do represent the daily average for any range of aerosol optical thicknesses or particle size (described there by the Ångström exponent). However in locations close to aerosol sources the daily cycle may be significant. Capo Verde is the closest maritime measurements to the African sources and was shows by Smirnov et al 2002] to have a diurnal cycle <5% of the optical thickness. Figure 16 tests this relationship. The AERONET data here are monthly averaged using measurements throughout the day while the MODIS data are centered on 10:30 am local time. Though some differences are due to spatial inhomogeneity or differences of AERONET to MODIS, on annual average MODIS is higher than AERONET by 4% in 2001 and lower than AERONET by 5% in 2002.

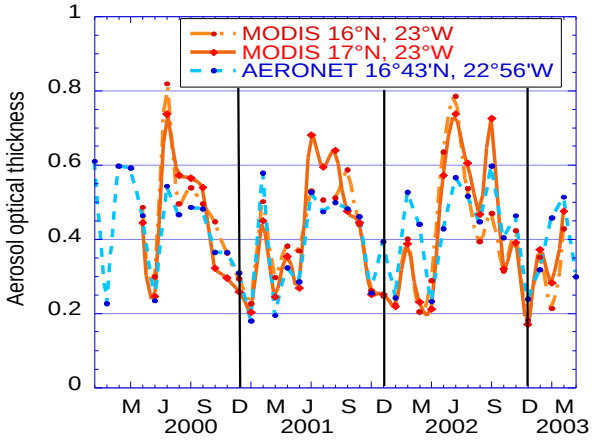

Fig.16: Monthly averages of the aerosol optical thickness measured by AERONET in Capo Verde and derived from MODIS around the location of the sunphotometer over the ocean. For the 2 full years of operation the MODIS optical thickness was 0.40-0.42 and AERONET was 0.39-0.43. The MODIS data are from Terra at ~ 10:30 am local time, the AERONET data are averaged on the daily hours. The AERONET level 1.0 data are used with only partial cloud screening due to possible screening of heavy dust with the accompanied clouds. Both data sets show similar seasonal cycle of the aerosol with maximum in the June-Sept time frame.

6. Conclusions

The interest in desert dust research and its effects on climate, ocean and land productivity, air pollution and atmospheric chemistry increased exponentially in the last 30 years, bringing abundant information on the dust optical/physical, and chemical properties. Already in the early works of Prospero and Carlson, the importance of satellite data in mapping the extent of the dust spread and transport was recognized and they were coupled with ground based and aircraft samplings to estimate the rate of dust emission transport and deposition.

The recent introduction of data from the MODIS instrument flown on Terra and Aqua introduces a new instrument with important capability for quantitative dust measurements. MODIS accuracy and spectral sampling across the solar spectrum, together with several years of dust remote sensing from the ground by AERONET, allows accurate measurements of the aerosol optical thickness and distinction between anthropogenic aerosol, dominated by fine sub-micron particles and dust or maritime aerosol with large fraction of coarse supermicron particles.

We reported here calculations of the dust monthly and annual transport from Africa and deposition in the Atlantic Ocean. The analysis reveals on a regional scale (fig. 5) the large fraction of biomass burning smoke imbedded in the dust in the winter months (45% smoke & 55% dust in Dec.-March) due to savanna fires in the Sahel, with purer dust (14% smoke, 86% dust) transported from Africa in the summer months (June-September).

The peculiar monthly oscillation of the dust transport with maxima and minima regularly oscillating between January and June was found to be easily explainable with similar oscillations of the monthly average wind westward component. The correlation of the wind with the dust column concentration is 82% (fig 11). The winds selection at 3-5 km in May-Oct. and 0-1 km in Nov. based on the literature, was reaffirmed using a similar correlation between winds and dust from AERONET data in Capo Verde (fig 9).

The results (fig. 6) confirm the migration of the dust center of gravity from close to the equator in the January to 20°N in September and back to the equator in December. In December-March dust is transported across the Atlantic Ocean to the Amazon Basin both below and above the equator. The 45 tg of dust that arrive to the Amazon, much larger than in the analysis of *Swap et al.* [1996] may explain the paradox described by *Swap et al.* [1996] between the need of nutrition by the Amazon forest and the source of the nutrition – the Saharan dust.

The annual dust deposition in 2001 of 120 tg derived from the MODIS analysis is comparable with the analysis of GOCART for the same year of 140 tg, and falls in between the 95 tg found by the *Gao et al.* [2003] model for particles <6 μm and 210 for particles ≤12 μm. *Prospero et al.* [1996] suggested for the general climatology 170 tg. Maximum deposition occurs in the summer, less is deposited in the fall and minimum deposition occurs in the spring and winter. This annual cycle agrees with the *Ginoux et al* GOCART model and to a large degree also with the *Gao et al.* [2001, 2003] models. The inter-annual variation between 2000 and 2003 was found to be very small in the MODIS data (fig 8).

APPENDIX: Dust mass to optical thickness ratio:

The dust mass column concentration is calculated from the optical thickness, using the following definition of the ratio of the dust mass to optical thickness, integrating on the size distributions:

$$M_{dust} / \tau_{dust} = (\rho 4\pi/3)\int r^3 n(r)dr \,/\, \pi\int Q(r) r^2 n(r)dr \qquad (A1)$$

where n(r) is the particle size distribution, Q~2.2 for the dust effective radius of 1.7 to 2.0 μm (size parameter X~20) obtained, respectively, from inversion of AERONET data [*Tanré et al.*, 2001] and measured in situ [*Maring et al*., 2003, referred here as M03]. Calculations by the GOCART model *[Ginoux et al.*, 2001, 2003] and by the model of *Gao et al.* [2003] show volume mean radius of 1.3 to 1.8 μm. Assuming Q is constant for dust, the ratio of the integrals in eq. 5 is the effective radius, therefore:

$$M_{dust} / \tau_{dust} = 1.33 \rho R_{eff}/Q \qquad (A2)$$

The specific weight is reported as ρ=2.0 gr/cm^3 by M03 and ρ=2.6 gr/cm^3 by *Haywood et al* [2003]. *Haywood et al* [2003] measured average extinction efficiency of 0.37 cm^3/gr, corresponding to M/τ_{dust} =2.7 gr/m^2. Note that the set of parameters taken from M03: of ρ=2.0 gr/cm^3 , R_{eff}=2 μm Q=2 gives the same value of M/τ_{dust} =2.7 gr/m^2. Also *Haywood* et al. [2003] ρ=2.6 gr/cm^3, combined with AERONET R_{eff}=1.7 μm and Q=2.2 also gives M/τ_{dust} =2.7 gr/m^2. Therefore M/τ_{dust} =2.7 gr/m^2 is the popularly selected ratio used here. Using Monte Carlo calculations for uncertainty of 10% in ρ and R_{eff} and 5% in Q we get:

$$M_{dust} = 2.7[\tau(0.9-f)/0.4 - \tau_{maritime}] \quad gr/m^2 \qquad (A3)$$

Several authors reported measurement of the extinction or scattering efficiency derived from the ratio of the extinction or scattering coefficient to the dust mass. *Moulin et al.*, [1997b] reviewed dust models giving 0.6-0.8 m^2/gr, corresponding to M/τ of 1.2-1.7 gr/m^2. *Chin et al.* [2002] used also 0.8 m^2/gr in their dust calculations. M03 derived 0.5 m^2/gr near Africa and inferred 0.6 m^2/gr in Barbados from measurements of *Li et al.* [1996], corresponding to M/τ of 2.0 and 1.7 gr/m^2, Dulac et al. noted the large uncertainty in the value and used 1.3 gr/m^2 somewhat lower than the values used here. On the other hand *Carlson* (1979) used a higher value of M/τ=3.6 gr/m^2. The small reduction in dust size from the African coast to the Caribbean suggest reduction of M/τ across the Atlantic. Since the magnitude of the reduction is 15% or smaller, and smaller than uncertainty the in M/τ, we did not include it in the calculations.

The uncertainties in the mass calculations, ΔM_{dust}, are due to errors in: M/τ ratio of ±0.4 gr/m^2, the regionally average total optical thickness - $\Delta\tau/\tau$ =±10% [*Remer et al.*, 2002], the fraction [(0.9−f)/0.4] of ±10%, and an error in the marine optical thickness - $\Delta\tau_{marit}$=±0.005. Monte Carlo calculations give total error of ±32% to ±30% for aerosol optical thickness of 0.2 and 0.4 respectively. These two optical thicknesses correspond to the regional average dust optical thickness and to the center of the dust respectively.

References

Alpert P, Krichak S. O, Tsidulko M, et al., A dust prediction system with TOMS initialization, Mon. Weather Rev. 130 (9): 2335-2345, 2002

Alpert, P., Y. J. Kaufman, Y. Shay-El et al., 1998; Quantification of Dust-Forced heating of the Lower Troposphere. *Nature, 395*, 367-370.

Barnes W. L., T .S. Pagano, and V.V. Salomonson, Pre-launch characteristics of MODIS on EOS-AM1, *IEEE Trans. Geosci., Rem. Sens., 36*, 1088-1100, 1998

Cakmur R. V., R. L. Miller and I. Tegen, A comparison of seasonal and interannual variability of soils dust aerosols over the Atlantic Ocean as inferred by the TOMS AI and AVHRR AOT retrievals. *J. Geophys. Res., 106*, D16, 18287-18303, 2001.

Carlson, T. N., Atmospheric turbidity in Saharan dust outbreaks as determined by analysis of satellite brightness data, *Monthly Weather Rev., 107*, 322335, 1979

Carlson, T. N. and J.M. Prospero, The large scale movement of Saharan air outbreaks over the Northern equatorial Atlantic, *J. Appl, Meteor., 11*, 283-297, 1972

Chiapello, I., G. Bergametti, L. Gomes, et al., An additional low layer transport of Sahelian and Saharan dust over the North-Eastern Tropical Atlantic, Geophys. Res. Lett., 22, 3191-3194, 1995.

Chiapello, I. and C. Moulin, TOMS and METEOSAT satellite records of the variability of Saharan dust transport over the Atlantic during the last two decades (1979-1997), Geophys. Res. Lett., 29, doi: 10.1029/2001GL013767, 2002.

Chiapello, I., J. M. Prospero, J. R. Herman, and N. C. Hsu, Detection of mineral dust over the North Atlantic Ocean and Africa with the Nimbus 7 TOMS, *J. Geophys. Res., 104*, 9277-9292, 1999a

Chiapello, I., G. Bergametti, B. Chatenet et al., Contribution of the different aerosol species to the aerosol mass load and optical depth over the northeastern tropical Atlantic, J. Geophys. Res., 104, 4025-4035, 1999b.

Chin, M *et al*., Tropospheric aerosol optical thickness from the GOCART model and comparisons with satellite and Sun photometer measurements, *J. Atmos. Sci.* 59, 461-483, 2002.

Dentener, F. J., G. R. Carmichael, Y. Zhang, J. Lelieveld, and P. J. Crutzen, Role of mineral aerosol as a reactive surface in the global troposphere, J. Geophys. Res., 101, 22,869-22,889, 1996.

Dubovik, O. *et al.* Variability of absorption and optical properties of key aerosol types observed in worldwide locations. *J. Atmos. Sci.* 59, 590-608, 2002.

Dubovik O, Holben BN, Lapyonok T, et al., Non-spherical aerosol retrieval method employing light scattering by spheroids, Geophys Res Lett 29, art. no. 1415 MAY 15, 2002.

Dulac F., D. Tanré, G. Bergametti et al., Assessment of the African airborne dust mass over the western Mediterranean sea using Meteosat data, J. Geophys. Res., 97, 2489-2506, 1992.

Erickson III, D. J., J. L. Hernandez, P. Ginoux et al., Atmospheric iron delivery and surface ocean biological activity in the Southern Ocean and Patagonia region, Geophys. Res. Lett., 30, 1609, doi:20.1029/2003GL017241, 2003.

Gao, Y.,S. M. Fan., J.L. Sarmiento, Aeolian iron input to the ocean through precipitation scavenging: a modeling perspective and its implication for natural iron fertilization in the ocean, J. Geophys. Res., 108, (D7) art. No. 4221 April, 2003.

Gao, Y., Y. J. Kaufman, D. Tanré, et al., Seasonal distributions of aeolian iron fluxes to the global ocean, Geophys. Res. Lett., 28,29–32, 2001.

Ginoux, P., M. Chin, I. Tegen, et al., Sources and distributions of dust aerosols simulated with the GOCART model, J. Geophys. Res., 106, 20,255–20,274, 2001.

Ginoux, P., J. M. Prospero, O. Torres, M. Chin, Long-term simulation of global dust distribution with the GOCART model: correlation with the North Atlantic Oscillation, *Environmental Modeling & Software*, doi:10.1016/S1364-8152(03)00114-2, 2003

Hastenrath S, On Climate Prediction In The Tropics, B Am Meteorol Soc 67 (6): 696-702 Jun 1986

Haywood, J., P. Francis, S. Osborne, et al., Radiative properties and direct radiative effect of Saharan dust measured by the C-130 aircraft during SHADE: 1. Solar spectrum, J. Geophys. Res., 108, 8577, 10.10129/2002JD002687, 2003.

Herman, J. R. *et al*. Global distribution of UV-absorbing aerosol from Nimbus-7/TOMS data. *J. Geophys. Res. 102*, 16911-16922, 1997.

Holben, B. N., J. Kandell and Y. J. Kaufman, Calibration of NOAA-11 AVHRR Visible and Near-IR bands. *Int. J. Rem Sens., 11*, 1511-1519, 1990.

Hsu, N.C. J.R. Herman. P.K. Bhartia et al., Detection of biomass burning smoke from TOMS measurements, *Geoph. Res. Let. 23*, 745-748, 1996.

Husar, R. B., J. M. Prospero, and L. L. Stowe, Characterization of tropospheric aerosols over the oceans with the NOAA advanced very high resolution radiometer optical thickness operational product, *J. Geophys. Res., 102*, 16,889-16,909, 1997.

Ignatov A. and L. Stowe Aerosol retrievals from individual AVHRR channels. Part I: Retrieval algorithm and transition from Dave to 6S radiative transfer model, *J. Atmos. Scie. 59*, 313-334, 2002

Jankowiak, I. And D. Tanré, Satellite climatology of Saharan dust outbreaks, J. of Climate, 5, 646-656, 1992

Kaufman, Y. J., A. Smirnov, B. N. Holben and O. Dubovik, Baseline maritime aerosol: methodology to derive the optical thickness and scattering properties, *Geophys. Res. Lett., 28*, 3251-3254, 2001

Kaufman, Y. J., D. Tanré, L. Remer, et al., Remote Sensing of Tropospheric Aerosol from EOS-MODIS Over the Land Using Dark Targets and Dynamic Aerosol Models, *J. Geophys. Res.*, 102, 17051-17067, 1997.

Kaufman, Y.J., B. N. Holben, D. Tanré, et al., Will aerosol measurements from Terra and Aqua polar orbiting satellites represent the daily aerosol abundance and properties? Geoph. Res. Let., 27, 3861-3864, 2000.

Kaufman, Y. J., D. Tanré and O. Boucher, A satellite view of aerosols in the climate system, Review for *Nature, 419*, 215-223, Sept. 12, 2002

Karyampudi, M. V., S. P. Palm, J. A. Reagan et al., Validation of the Saharan dust plume conceptual model using Lidar, METEOSAT, and ECMWF data, Bull. Amer. Meteor. Soc., 80, 1045-1076, 1999.

King, M. D., Y. J. Kaufman, D. Tanré, and T. Nakajima, Remote sensing of tropospheric aerosols from space: past, present and future. *Bull. of Meteor. Soc.. 80*, 2229-2259, 1999

King, M. D., W. P. Menzel, Y. J. Kaufman, et al, Cloud and aerosol properties, precipitable water, and profiles of temperature and humidity from MODIS. *IEEE Trans. Geosci. Remote Sens., 41*, 442-458, 2003.

Levin, Z., Ganor, E. & Gladstein, V. The effects of desert particles coated with sulfate on rain formation in the Eastern Mediterranean. *J. Appl. Meteor.* **35**, 1511-1523, 1996.

Li, X., H. Maring, D. Savoie, K. Voss and J.M. Prospero, Dominance of mineral dust in aerosol light scattering in the North Atlantic trade winds, *Nature, 380*, 416-419, 1996.

Maring H et al., Mineral dust aerosol size distribution change during atmospheric transport, JGR, 108(D19), 8592, doi:10.1029/2002JD002536, 2003

Martin, J. H., R. M. Gordon and S. E. Fitzwater, The case for iron, Limnology and Oceanography, 36, 1793-1802, 1991.

Martin, R. V., D. J. Jacob, R. M. Yantosca, M. Chin, and P. Ginoux, Global and regional decreases in tropospheric oxidants from photochemical effects of aerosols, J. Geophys. Res. 108, 4097, doi: 10.1029/2002JD002622, 2003.

Martins, J. V., D. Tanré, L.A. Remer, et al, MODIS Cloud screening for remote sensing of aerosol over oceans using spatial variability, Geophys. Res. Lett., 29(12),10.1029/2001GL013252, 2002.

Mishchenko M.I., Travis L.D., Kahn R.A., et al., Modeling phase functions for dustlike tropospheric aerosols using a shape mixture of randomly oriented polydisperse spheroids J. Geophys. Res., 102, 16831-16847, 1997

Moulin, C., C. E. Lambert, F. Dulac, and U. Dayan, Control of atmospheric export of dust from North Africa by the North Atlantic Oscillation, *Nature, 387*, 691-694, 1997a.

Moulin, C., F. Dulac, C. E. Lambert, et al, Long term daily monitoring of Saharan dust load over ocean using Meteosat ISCCP-B2 data, 12, accuracy of the data and validation using sunphotometer measurements, *J. Geophys. Res. 102*, 16959-19969, 1997b.

Pinker R. T., G. Pandithurai, B. N. Holben, et al., A dust outbreak episode in sub-Sahel West Africa *J. Geophys. Res. 106*, 22923-22930, 2001

Prospero J.M. and T. N. Carlson, Vertical and areal distribution of Saharan dust over the western equatorial North Atlantic ocean, J. Geophys. Res., 77, 5255-5265, 1972.

Prospero J.M. and R.T. Nees, Dust concentration in the atmosphere of the equatorial North Atlantic Possible relationship to Sahelian drought. *Science, 196*, 1196-1198, 1977.

Prospero, J.M., R.A. Glaccum and R.T. Nees.Atmospheric transport of soil dust from Africa to South America. Nature, 289:570-572, 1981.

Prospero, J. M., K. Barrett, T. Church, et al., Atmospheric deposition of nutrients to the North Atlantic basin, Biogeochemistry, 35, 27-73, 1996.

Prospero, J.M., P. Ginoux, O. Torres, et al., Environmental characterization of global sources of atmospheric soil dust identified with the nimbus 7 total ozone mapping spectrometer (TOMS) absorbing aerosol product, Reviews of Geophysics, 40, doi:10.1029/2000RG000095, 2002.

Prospero, J. M., Long term measurements of the transport of African mineral dust to the Southern US: Implications for regional air quality. *J. Geophys. Res.* 104, 15917-15927, 1999.

Ramanathan, V. *et al.* The Indian Ocean Experiment: An integrated analysis of the climate forcing and effects of the great Indo-Asian haze. *J. Geophys. Res*. 106, 28371-28398, 2001.

Remer, L. A., D. Tanré, Y. J. Kaufman, et al., Validation of MODIS aerosol retrieval over ocean. Geophys. Res. Lett., 29 (12): art. no. 1618 JUN 15, 2002

Rosenfeld, D., Y. Rudich, & R. Lahav, Desert dust suppressing precipitation - a possible desertification feedback loop. *Proc. Nat. Academy Sci. 98*, 5975-5980, 2001.

Smirnov A, B. N. Holben, T. F. Eck, et al. Diurnal variability of aerosol optical depth observed at AERONET sites Geophys. Res. Lett., 29 (23): art. no. 2115 DEC 10 2002

Smirnov A, B. N.Holben, T. F. Eck, et al., Effect of wind speed on column aerosol optical properties at Midway Island Geophys. Res. Lett.,in press 2003

Swap R, M. Garstang, S. Greco, et al., Saharan dust in the Amazon basin, *Tellus Series B-Chemical and Physical Meteorology, 44*, 133-149, 1992.

Swap R, Ulanski S, Cobbett M, Garstang M, Temporal and spatial characteristics of Saharan dust outbreaks, *J. Geophys. Res., 101*, 4205-4220 Feb. 1996.

Stanhil, G., The growth of climate change science: a scientometric study, *Climate Change, 48*, 515-524, 2001.

Tanré D, Devaux C, Herman M, et al., Radiative properties of desert aerosols by optical ground based measurements at solar wavelengths, *J Geophys. Res. 93*, 14223-14231, 1988

Tanré, D., M. Herman and Y.J. Kaufman,, Information on aerosol size distribution contained in solar reflected radiances. *JGR-Atmospheres, 101*, 19043-19060, 1996.

Tanré, D., Y. J. Kaufman, M. Herman and S. Mattoo, Remote sensing of aerosol over oceans from EOS-MODIS, *J. Geophys. Res, 102*, 16971-16988. 1997

Tanré, D., L.R. Remer, Y.J. Kaufman, et al., Retrieval of Aerosol Optical Thickness and Size Distribution Over Ocean from the MODIS Airborne Simulator during Tarfox, *J. Geophys. Res, 104*, 2261-2278, 1999.

Tanré, D., Y. J. Kaufman, B.N. Holben, et al., Climatology of dust aerosol size distribution and optical properties derived from remotely sensed data in the solar spectrum, *J. Geophys. Res, 106*, 18205-18217, 2001.

Tegen, I. and I. Fung, Modeling of mineral dust in the atmosphere - sources, transport, and optical-thickness. *J. Geophys Res. 99*, 22897-22914, 1994.

Torres, O., et al., A long-term record of aerosol optical depth from TOMS observations and comparison to AERONET measurements, *J. Atmos. Scie*., 59: 398-413 (2002)

Y. J. Kaufman (kaufman@climate.gsfc.nasa.gov), Tel 301-614-6189; Fax 301-614-6307